Int J Adv Manuf Technol (2018) 95:2767–2782
https://doi.org/10.1007/s00170-017-1249-2

ORIGINAL ARTICLE

Micro-flank milling forces considering stiffness of thin-walled parts

Jie Yi[1] · Xibin Wang[2] · Li Jiao[2] · Mingxin Li[3] · Junfeng Xiang[1] · Pei Yan[2] · Shiqi Chen[1]

Received: 7 May 2017 / Accepted: 24 October 2017 / Published online: 28 November 2017

Abstract A novel micro-flank milling force prediction model is developed in this study by considering the deflection of tool and workpiece, tool run-out, and material strengthening effects during the flank milling of thin-walled parts. The model of the cutting tool applied in this study is closer to the actual structure and its deflection model is established based on Euler Bernoulli cantilever beam theory under mesoscale. The values of the workpiece deflection are obtained with an online Keyence LK-H020 laser sensor. The Johnson−Cook constitutive model is adopted to estimate the flow stress σ_{JC}, which takes in consideration the effects that strain-hardening, strain-rate, and thermal softening have on the flow stress. The mechanistic model is validated by a series of micro-thin-wall experiments with a two-flute KENNA micro-milling cutter as tool and Ti-6Al-4V titanium alloy as workpiece material. Experimental results illustrate that the proposed model performs well for the micro-flank milling forces in the *x*-direction, with an average error of 4.153%, while the error in the *y*-direction is slightly larger at 4.458%.

Keywords Micro-flank milling force model · Thin-walled parts · Deflection of tool and workpiece · Ti-6Al-4V titanium alloy

✉ Li Jiao
jiaoli@bit.edu.cn

Jie Yi
825762984@qq.com

Xibin Wang
cutting0@bit.edu.cn

Mingxin Li
mingxinli1994@163.com

Junfeng Xiang
xiang_junfeng@126.com

Pei Yan
pyan@bit.edu.cn

Shiqi Chen
851085275@qq.com

[1] School of Mechanical Engineering, Beijing Institute of Technology, Beijing 100081, China

[2] Key Laboratory of Fundamental Science for Advanced Machining, Beijing Institute of Technology, Beijing 100081, China

[3] School of Xu Teli, Beijing Institute of Technology, Beijing 100081, China

1 Introduction

Micro-milling has become a widely utilized process in the tool and die industry for acquiring high-dimensional accuracy and good surface finish for the production with 3D micro-features [1]. With the development of a broad spectrum of products [2], highly accurate miniaturized complex components made of a variety of difficult-to-machine materials have played a key role under mesoscale. Because of several reasons, such as the small size of machined parts and its tiny feed rate, the machining mechanism of mesoscale milling is different from that of macro-scale. Such situations, namely size effects, have a great influence on machining accuracy. The machining precision can be affected by a lot of error sources during multi-stage machining. All of these error sources result in difficulties in accuracy control. The present study focuses on thin walls because their features present a typical challenge to micro-milling and require very high tolerance [3]. Micro-milling forces are among the most fundamental and important parameters to be considered during the flank milling of thin-walled parts, especially considering using Ti-6Al-4V titanium alloy

as the thin wall material. As in Fig. 1, the purpose of this work is to analyze the micro-milling forces when flank milling thin walls abstracted from a micro-impeller.

So far, a lot of studies have used the mechanistic model to calculate the micro-milling forces during the micro-end milling process. Bissacco et al. [4] proposed a model to calculate the micro-milling forces based on the ratio of the uncut chip thickness to cutting edge radius. Park et al. [5] presented a mechanistic model of cutting forces by taking into account shearing and plowing dominant cutting regimes according to the tool edge radius effect. Malekian et al. [6] made a research on the mechanistic cutting force model for the plowing and shearing dominant regimes including tool run-out, dynamics, and elastic recovery of the material. Rodríguez and Labarga [7] developed an analytical force model for realistic micro-end milling by considering the eccentric deviation of the tool path, tool deflection, size effect, and the variation in the entry and exit angles of the tool. Tool run-out has significant effects on cutting force variation, which can lead to higher peak forces and uneven tool wear of the cutter. Hence, Jing et al. [8] provided that a run-out model must be included in a cutting force modeling to simulate accurate cutting force during micro-milling process. Mamedov et al. [9] developed comprehensive cutting force and deflection models from which the tool deflection in micro-end milling can be determined. In order to predict the general three-dimensional cutting force components, the related cutting edge radius size effect, tool run-out, tool deflection, and the exact trochoidal trajectory of tool flutes are considered and presented in the proposed analytical prediction model [10]. In order to avoid the numerical oscillations from differential model and to eliminate the influence of the ill-posed problem in calibration, Zhang et al. [11] proposed a new approach to calibrate the cutter radial run-out parameters from the continuous cutting force model with constant cutting coefficients. However, the researches on micro-milling forces above are all conducted on slot milling, without considering the influence of micro-thin-walled deflection.

The influence of material strengthening on micro-milling forces is one of the significant characteristics during the micro-machining process. Many efforts have been dedicated to the analytical modeling of cutting forces regarding material strengthening. Joshi et al. [12] presented a modified Johnson–Cook constitutive model by introducing the material length scale and effective strain gradient. Liu et al. [13] adopted this modified Johnson–Cook constitutive model to the finite element based micro-orthogonal cutting simulations, and the results showed that the strain gradient strengthening effect is prominent especially at small uncut chip thicknesses. Srinivasa and Shunmugam [14] presented a new methodology for predicting the cutting coefficients considering the edge radius and material strengthening effects. Zhou et al. [15] developed a novel comprehensive micro-end milling force prediction methodology considering factors including edge

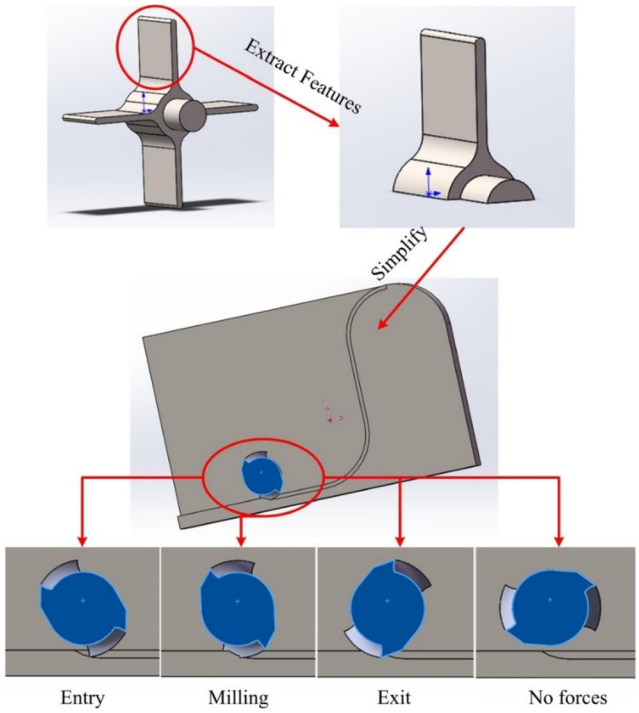

Fig. 1 Process of machining micro-thin wall derived from the micro-impeller

radius, material strengthening, varying sliding friction coefficients, and run-out. However, these studies do not consider the effect of the deflection of tool and workpiece on micro-milling forces.

In this work, a novel micro-end milling cutting force prediction model is presented by considering tool run-out, the material strengthening effect, and the effects of both the deflection of tool and workpiece during the flank milling thin-walled parts. The model of cutting tool is closer in resemblance to the actual structure and its deflection model is established based on the Euler Bernoulli cantilever beam theory. The thickness of the thin-wall-structured workpiece is no larger than 20% of its height or width, which can be considered as a thin plate model when applied to forces [16]. Since analytical solution of the deflection for a thin plate model under dynamic milling forces is incredibly difficult to obtain, so in this work, the model will utilize the deflection measurements of the thin-walled structure obtained by a Keyence LK-H020 laser sensor. In addition, the Johnson–Cook constitutive model is adopted to estimate the flow stress σ_{JC}, which includes the effects of strain hardening, strain rate, and thermal softening effects on the flow stress. The mechanistic model is validated by a series of micro-thin-wall experiments with a two-flute KENNA micro-end mill as tool and Ti-6Al-4V titanium alloy as material of the thin-walled workpiece. Experimental results illustrate that the proposed model performs well for the micro-milling forces. In the x-direction, the average error is 4.153%; error in the y-direction is slightly larger at 4.458%.

2 Theoretical model

2.1 Influence of tool run-out

Figure 2 depicts the simulation flow chart for predicting micro-milling forces. The Zhang and Wang [17] developed the instantaneous uncut chip thickness under the effect of tool run-out for micro-end milling as follows:

$$h_0 = f_z \sin\varphi + 2\rho\cos\left(\lambda - \phi_z - \frac{2\pi(i-1)}{N_t}\right) \quad (1)$$

where φ is the angular position of the cutting tool teeth, f_z is the feed per tooth, ρ is radial run-out length, λ is the run-out angle, N_t is the total number of cutting teeth of the cutter, i is the indicator of the current cutting flute, and ϕ_z is the radial lag angle which has been discussed by Yongqing W. and Haibo L. [18]

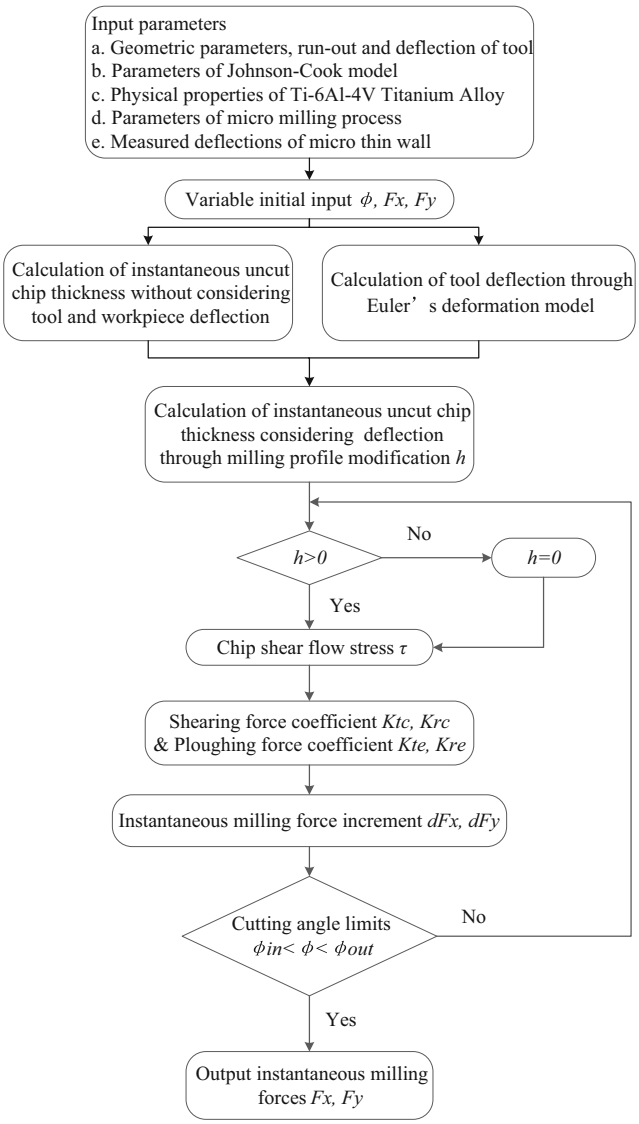

Fig. 2 Simulation flow chart for predicting micro-milling forces

2.2 Influence of tool deflection and workpiece deflection

In macro-normal milling process, the rigidity of milling cutter and machine tool is high, so the elastic deflection of milling cutter is usually negligible. However, in the micro-milling process, the milling cutter whose diameter of 0.1–1 mm, which is much smaller than the diameter of the cutter bar of 3–5 mm, is much more prone to the negative effects of poor rigidity on the cutter tooth's trajectory, the surface shape error, and the milling surface accuracy. Furthermore, the deflection of the micro-milling cutter has a direct impact on the thickness accuracy of the machined thin wall. Therefore, the model of micro-milling cutter deflection should be established in micro-machining process. In this proposed model, the tool deflection is only considered in the direction normal to the micro-milling cutter, due to the negligibility of the forces applied on the tool in the direction parallel of the micro-milling cutter during flank milling. The Euler Bernoulli beam equation is accustomed to interpret the tool deflection of three-section cantilever beam which characterizes the ball nose micro-end mill studied in this model. The three sections of the micro-end mill consist of a shank, a conic section, and a neck which includes a cutting section. Figure 3 illustrates the approximated geometry of micro-end mill.

Micro-end milling deflection is caused by a force F produced by the milling action occurring near the tip of the tool. The equation generated by the relationship between bending moment and bending deflection is:

$$EI(z)\delta(z)'' = -M \quad (2)$$

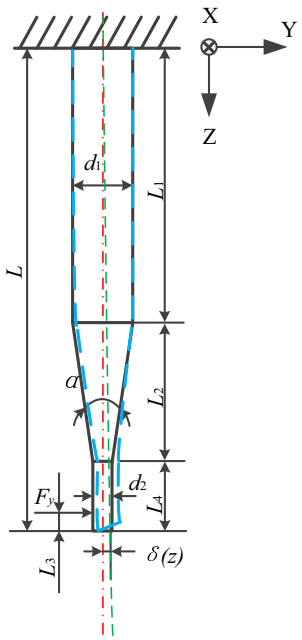

Fig. 3 The approximate geometry of micro-end mill

where the bending moment M is calculated from the equilibrium conditions obtained as follows:

$$M = -F(L-z). \tag{3}$$

E is the modulus of elasticity of tungsten carbide.

An expression for the second moment of area for the circular cross-section of the milling cutter is as follows:

$$I(z) = \frac{\pi d^4(z)}{64}. \tag{4}$$

The diameter of micro-end milling cutter, d is the difference for each of the three sections of the tool, depending on a length variable z as follows:

$$z = \begin{cases} d_1 & z\in[0, L_1] \\ d_1 - 2\tan\left(\frac{\alpha}{2}\right)(z-L_1) & z\in[L_1, L_1+L_2] \\ d_2 & z\in[L_1+L_2, L-L_3] \end{cases} \tag{5}$$

where $L_2 = \frac{d_1-d_2}{2\tan\frac{\alpha}{2}}$, $L = L_1 + L_2 + L_4$.

Double integrate Eq. (1) to obtain deflection curves for the three sections as follows:

$$\delta(z) = \begin{cases} -\frac{F}{6EI_1}z^3 + \frac{FL}{2EI_1}z^2 + B_1 z + B_2 & z\in[0, L_1] \\ \frac{a(-3mz+mL-2n)}{6m^3(mz+n)^2} + B_3 z + B_4 & z\in[L_1, L_1+L_2] \\ -\frac{F}{6EI_3}z^3 + \frac{FL}{2EI_3}z^2 + B_5 z + B_6 & z\in[L_1+L_2, L-L_3] \end{cases} \tag{6}$$

where $a = \frac{64F}{E\pi}$, $m = -2\tan\frac{\alpha}{2}$, $n = d_1 + 2L_1\tan\left(\frac{\alpha}{2}\right)$.

Constants of integration, B_1 to B_6, are calculated based on boundary conditions, where the micro-end milling cutter (a) is assumed to be rigidly mounted into a tool holder, and the values of slopes and deflections (b) between sections are continuous [19].

The tool deformation calculated with the equations above can alter the instantaneous uncut chip thickness by alternating the pass the milling cutter takes. Figure 4 illustrated the micro-flank milling progress. In Fig. 4b, ⊙O represents the cross-sectional profile the cutter at the rotational angle of φ_a; ⊙O1 represents the cross-sectional profile when the next flute is engaged in cutting, without considering tool deformation; ⊙O′1 represents the cross-sectional profile when the next flute is engaged in cutting, considering tool deformation.

The instantaneous uncut chip thickness h_1 which corresponds with the cross-sectional profile of ⊙O′1 can be calculated using the geometric relation in Fig. 4b and the instantaneous uncut chip thickness h_0 which corresponds to the cross-sectional profile of ⊙O. Define radius of ⊙O as R,

$$R = \frac{d_2}{2} \tag{7}$$

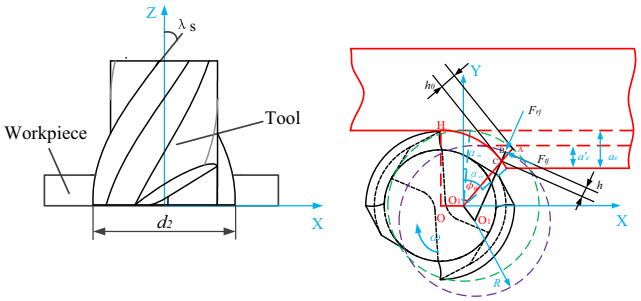

Fig. 4 Micro-flank milling progress. **a** Details of helical two-flute end-mill. **b** Single tooth and mechanistic predicted model

$$\varphi_a = \tan^{-1}\frac{R-a_e}{R-h_0}. \tag{8}$$

According to the trigonometry law of cosines,

$$\overline{CO_1'}^2 = (R-h_0)^2 + d_x^2 + d_y^2 - 2 \times \sqrt{d_x^2+d_y^2}(R-h_0)\cos\left(\pi - \varphi_a - \tan^{-1}\frac{d_x}{d_y}\right) \tag{9}$$

where d_x and d_y represent the absolute value of the tool deformation in the x- and y-directions accordingly. Thus, the instantaneous uncut chip thickness with tool deformation in consideration can be expressed with the following equation:

$$h_1 = R - \overline{CO_1'}. \tag{10}$$

In the process of machining micro-thin wall, the deformation of workpiece is difficult to calculate using analytical methods. Therefore, the deflection of workpiece is incorporated into our proposed model using experimental measurements obtained by Keyence LK-H020 laser sensor. The section of the workpiece subject to milling in the model is fixed to the bulk of the workpiece on two sides.

Considering micro-milling, the elastoplastic deformation of the Ti-6Al-4V workpiece is approximately opposite the chip thickness direction. The workpiece deformation is denoted as d_w. The instantaneous uncut chip thickness while considering both tool deformation and chip deformation can be taken as denoted by $\overrightarrow{h}$.

$$\overrightarrow{h} = \overrightarrow{h_1} - \overrightarrow{d_w} \tag{11}$$

Table 1 Ti-6Al-4V Johnson–Cook constitutive model parameters for purposed micro-milling model [23]

A (MPa)	B (MPa)	C	m	n	$\dot{\varepsilon}_0$ (s^{-1})
782.7	498.4	0.028	1	0.28	10^{-5}

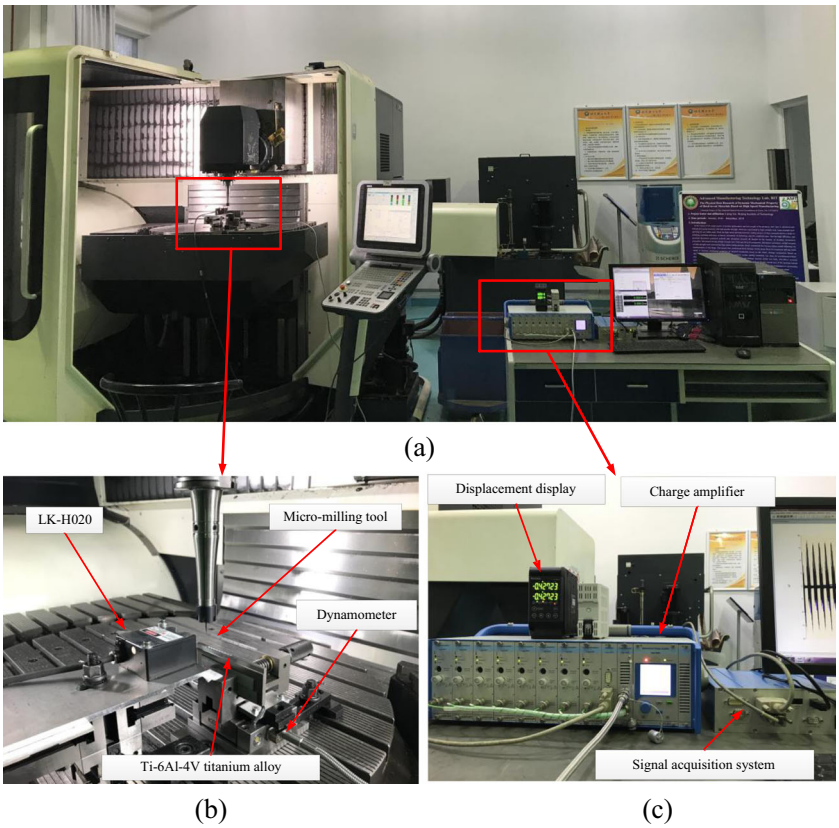

Fig. 5 Experimental set-up. **a** Actual set-up for micro-end milling and measurement. **b** Micro-milling Ti-6Al-4V titanium alloy. **c** Measuring micro-milling force and deflection of thin wall

2.3 Prediction of the micro-flank milling forces

As shown in Fig. 4a, the Cartesian coordinate system of a helical two-flute micro-end mill is established. The origin point is located at the center of the micro-end mill tip circumference. The x-axis is designated along the feed direction and the y-axis normal to the machined surface of the workpiece. The z-axis is perpendicular to both the x- and y-axes. When modeling the micro-flank milling forces, the micro-end mill is usually divided into a number of small differential oblique cutting elements along the z-axis, according to Zhou et al. [15]. The thickness of each element can be derived by the angular step of each flute.

$$dz = \frac{d\varphi \cdot d_2}{2\tan\lambda_s} \tag{12}$$

where d_2 is the tool diameter at the line of contact with the workpiece, λ_s is the helix angle of the tool edge.

A component of the micro-flank milling forces acted on these elements is the result of the plowing stress caused by the round edge of the cutter and the other one is the result of the shearing stress caused by the cutting process. Omitting the axial force of the cutter, the micro-flank milling forces exerted on the differential elements comprised of these two components can be expressed as follows:

$$\begin{cases} dF_t(\varphi) = (K_{te} + K_{tc}h(\varphi))dz \\ dF_r(\varphi) = (K_{re} + K_{rc}h(\varphi))dz \end{cases} \tag{13}$$

K_{te} and K_{re} are the plowing force coefficients, $K_{tc}$and K_{rc} are the shearing force coefficients, and $h(\varphi)$ is the instantaneous uncut chip thickness. Decompose the differential micro-flank

Table 2 Ti-6Al-4V physical characteristics

Parameters	Value	Parameters	Value
Density (kg/m^3)	4500	Yield strength (MPa)	820
Fusing point ($^\circ$C)	1649	Elastic modulus (GPa)	113.8
Thermal conductivity (W/(m K))	7.2	Poisson's ratio	0.342
Tensile strength limit (MPa)	950	Specific heat capacity (J/(kg$^\circ$C))	678
Elongation (%)	14.0		

Table 3 Ti-6Al-4V chemical compositions

Chemical element	C	Fe	N	O	AL	V	H	Ti
Content (%)	1	3	0.5	0.2	5.5–6.8	0.35–0.45	0.15	Rest

milling forces on an orthogonal basis, differential forces on x- and y-axes are as follows:

$$\begin{cases} dF_x = \dfrac{d_2}{2\tan\lambda_s}[K_{te}\cos\varphi + K_{re}\sin\varphi + (K_{tc}\cos\varphi + K_{rc}\sin\varphi)h]d\varphi \\ dF_y = \dfrac{d_2}{2\tan\lambda_s}[-K_{te}\cos\varphi + K_{re}\sin\varphi + (-K_{tc}\cos\varphi + K_{rc}\sin\varphi)h]d\varphi \end{cases} \tag{14}$$

The John–Cook model of oblique cutting developed by Zhou et al. [15] is adapted in this model. Accordingly, the shearing force coefficients K_{tc} and K_{rc} can be calculated by the following equations:

$$\begin{cases} K_{tc} = \dfrac{\tau}{\sin\phi_n} \dfrac{\cos(\beta_n - \alpha_n) + \tan i \tan\eta_c \sin\beta_n}{\sqrt{\cos^2(\phi_n + \beta_n - \alpha_n) + \tan^2\eta_c \sin^2\beta_n}} \\ K_{rc} = \dfrac{\tau}{\sin\phi_n \cos i} \dfrac{\sin(\beta_n - \alpha_n)}{\sqrt{\cos^2(\phi_n + \beta_n - \alpha_n) + \tan^2\eta_c \sin^2\beta_n}} \end{cases} \tag{15}$$

where τ represents the shear flow stress on the shear plane, i represents the inclination angle, η_c represents the chip velocity angle measured on the rake face, β_n represents the normal friction angle, α_n represents the normal rake angle, and ϕ_n represents the normal shear angle. The inclination angle i is equal to the helix angle λ_s, while according to Stabler's rule it is also approximately equal to the chip velocity angle η_c.

When the instantaneous uncut chip thickness equal or less than the edge radius, the effective rake angle affecting the machining process is more negative than the nominal rake angle. So, the average effective rake angle model has been established to analyze the influence of the edge radius on the micro-milling process. In this model, the effective rake angle α_e is estimated by the average effective rake angle as follows [15]:

$$a_e = \begin{cases} \arctan\left(-\dfrac{\sqrt{\left(2 - \dfrac{\varsigma h}{r_e}\right)} - \sin\theta_f}{\dfrac{\varsigma h}{r_e} - 1 + \cos\theta_f} \right), & \dfrac{h}{r_e} < 1 + \sin\alpha \\ \arctan\left(\dfrac{\left(\dfrac{\varsigma h}{r_e} - 1\right)\tan\alpha_n - \sec\alpha_n + \sin\theta_f}{\dfrac{\varsigma h}{r_e} - 1 + \cos\theta_f} \right), & \dfrac{h}{r_e} \geq 1 + \sin\alpha \end{cases} \tag{16}$$

where α represents the normal rake angle, θ_f stands for the separation angle which is 37.6° according to Basra and Misra [20], ς is taken as 1.5 in this model [21], and r_e is the edge radius of the micro-milling cutter. The normal rake angle α_n can be replaced by the effective rake angle α_e.

Based on momentum equilibrium analysis, the normal friction angle β_n can be expressed as follows:

$$\tan\beta_n = \frac{\xi + 2}{4(\xi + 1)} \frac{\sin 2(\phi_n + \beta_n - \alpha_n)}{\cos^2\beta_n} \left\{ \xi \left\{ 1 - \left[\frac{\xi + 2}{4\mu(\xi + 1)} \frac{\sin 2(\phi_n + \beta_n - \alpha_n)}{\cos^2\beta_n} \right]^{\frac{1}{\xi}} \right\} + 1 \right\} \tag{17}$$

where ξ is the exponential constant of the pressure distribution and set with 3, and μ represents the sliding friction coefficient. With a low cutting speed of 28.26 m/min, the sliding friction coefficient is considerably high at 0.8 on the tool-chip interface.

Substituting Eq. (16) into Eq. (17), the Newton-Raphson iterative method can be applied to solve β_n in Eq. (17) and obtain an array of solutions under different cases of t. In addition, the technique of polynomial fitting can be utilized to form an explicit function for β_n of t.

With α_n and β_n both functions of h, the normal shear angle for this cutting model ϕ_n can also be expressed as a function of h by adopting the Merchant model as follows:

$$\phi_n = C_1 - C_2(\beta_n - \alpha_n) \tag{18}$$

where C_1 is taken as 0.9532 and C_2 is taken as 0.5.

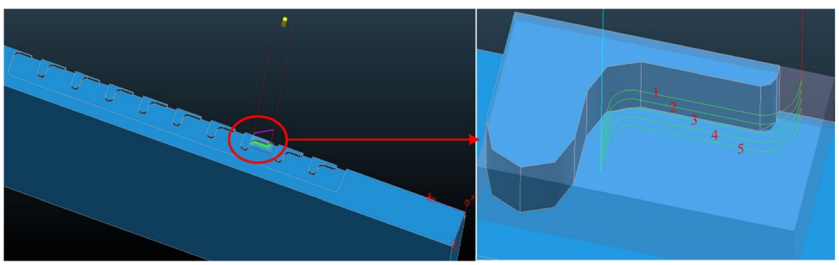

Fig. 6 Tool trajectory of delamination micro-milling thin wall

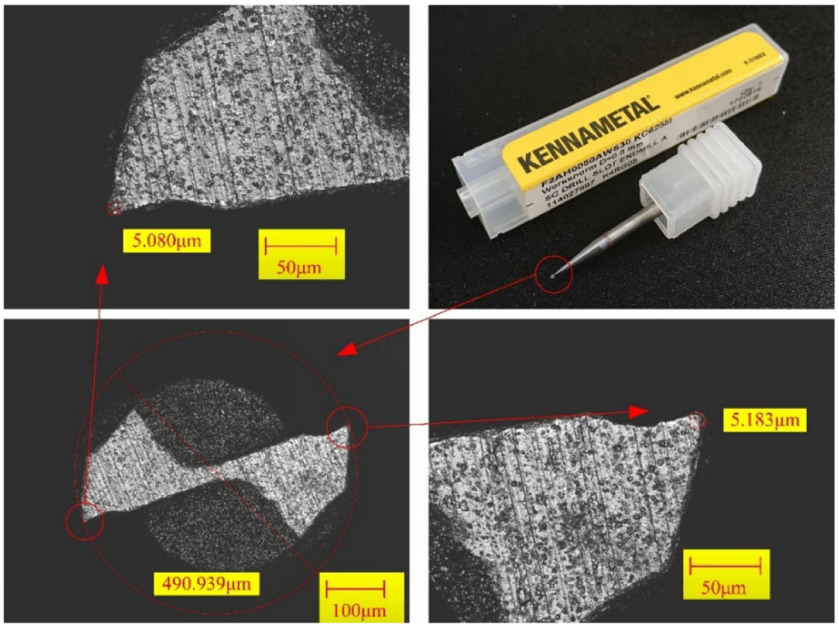

Fig. 7 Optical zoom of micro-end milling cutter (KENAMETAL)

In this model, the plowing force coefficients K_{te} and K_{re} are determined by adopting the analytical model developed by Abdelmoneim and Scruttron [22]:

$$K_{te} = r_e\tau\left(\frac{2\theta_0}{\cos\theta_0} + \pi\sin\theta_0\tan\theta_0\right) \tag{19}$$

$$K_{re} = r_e\tau\left(2\sqrt{3}\sin\theta_0\right) \tag{20}$$

where θ_0 is the stagnation point angle:

$$\theta_0 = \frac{\pi}{4} - \frac{\beta_n}{2}. \tag{21}$$

2.3.1 Estimation of shear stress and material strengthening effect

The Johnson–Cook constitutive model which contains the influence of strain hardening, strain rate, and thermal softening effects on the flow stress is adopted to estimate the flow stress σ_{JC}. It can be given as follows:

$$\sigma_{JC} = (A + B\varepsilon^n)\left(1 + C\ln\left(\frac{\dot{\varepsilon}}{\dot{\varepsilon}_0}\right)\right)\left(1 - \left(\frac{T - T_r}{T_m - T_r}\right)^m\right). \tag{22}$$

The Johnson–Cook constitutive model parameters applied for the calculation of the flow stress contain: A is the initial yield strength, B is the strain hardening coefficient, $\dot{\varepsilon}_0$ is the reference plastic strain rate, n and m are the strain hardening coefficients, separately, and C is the strain rate coefficient. Their values are taken in accordance with the high temperature and high strain rate involved at the contact region of the Ti-6Al-4V material during milling. In addition, the values of these parameters are given in Table 1.

Other parameters included in the calculation of the flow stress include: T_m, the material melting temperature is 1604 °C as for Ti-6Al-4V, T_r, the room temperature is given as 20 °C, ε, the equivalent plastic strain, and $\dot{\varepsilon}$, the equivalent plastic strain-rate. In orthogonal cutting, when both the plastic strain and strain rate are on the main shear plane as in this case, their expressions are expressed as follows:

$$\varepsilon = \frac{\cos\alpha_n}{2\sqrt{3}\sin\phi_n\cos(\phi_n - \alpha_n)} \tag{23}$$

Table 4 Basic parameters of micro-milling tool

Parameters	Value
Shrank diameter d_1 (mm)	3
Cutting diameter d_2 (mm)	0.5
Shrank length L_1 (mm)	8
Neck length L_4 (mm)	1
Cutting length L_3 (mm)	0.1
Conic angle α (°)	30
Average edge radius r_β (µm)	5.132
Elastic modulus (GPa)	707
Maximum run-out ρ (µm)	1.026

Table 5 Mechanical parameters of Kistler dynamometer 9119AA2

Measuring range	Threshold	Sensitivity		Natural frequency		
F_x, F_y, F_z		F_x, F_z	F_y	$f_n(x)$	$f_n(y)$	$f_n(z)$
kN	N	pC/N	pC/N	kHz	kHz	kHz
− 4 … 4	< 0.002	− 26	− 13	4.3	4.6	4.4

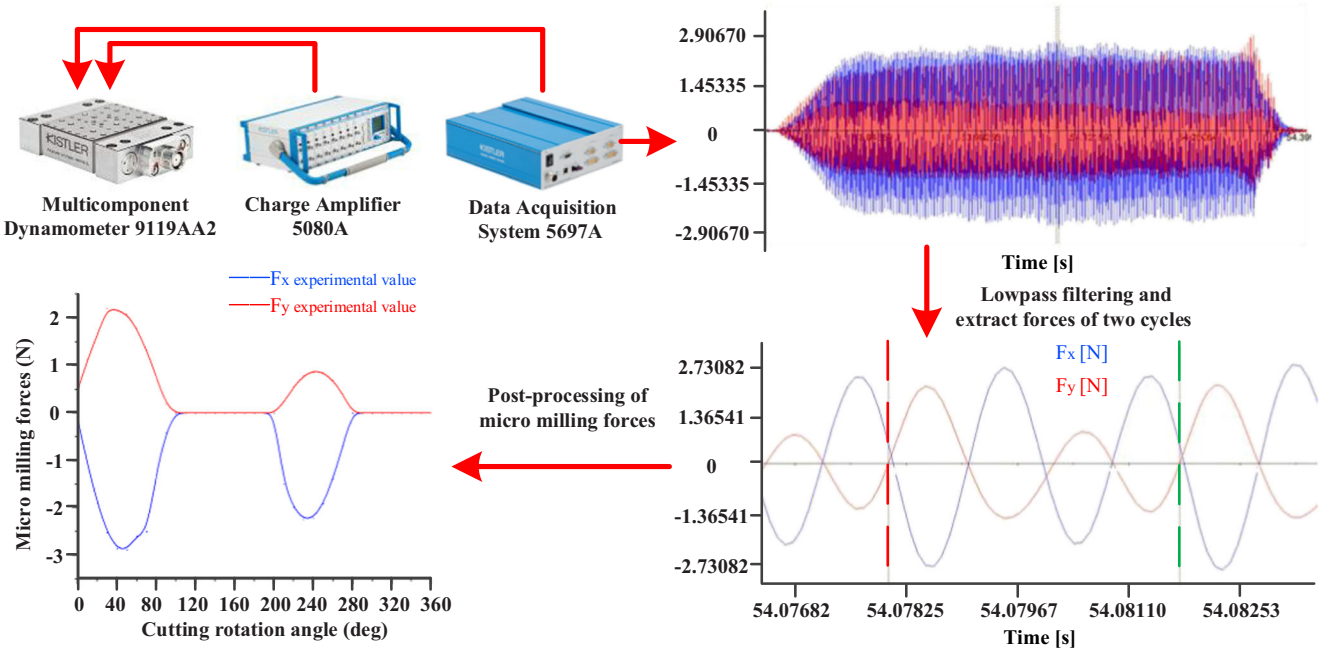

Fig. 8 Post-processing of micro-flank milling forces

$$\dot{\varepsilon} = \frac{2V\cos\alpha_n}{\sqrt{3}h_p\cos(\phi_n - \alpha_n)} \tag{24}$$

where h_p is the primary shear zone thickness which is approximately to be $0.5h$ [24].

The temperature T on the shear plane is determined by the equation as follows:

$$\int_{T_0}^{T} \frac{\rho_m C_p}{\left(1-\left(\frac{T-T_r}{T_m-T_r}\right)^m\right)} dT = \beta_T (A + B\varepsilon^n)\left(1 + C\ln\left(\frac{\dot{\varepsilon}}{\dot{\varepsilon}_0}\right)\right). \tag{25}$$

where ρ_m, the density of the material Ti-6Al-4V is 4500 kg/m^3; C_p, the specific heat is 678 J/(kg °C); β_T, the percentage of total shear deformation energy contributing to the temperature increase is assumed to be 0.9 [15].

Arranging Eq. (25), the expression for T can be simplified as follows:

$$T = T_m - e^R \tag{26}$$

where R is defined as follows:

$$R = \frac{\rho_m C_p \ln(T_m - T_r) - \beta_T (A + B\varepsilon^n)\left(1 + C\ln\left(\frac{\dot{\varepsilon}}{\dot{\varepsilon}_0}\right)\right)}{\rho_m C_p}. \tag{27}$$

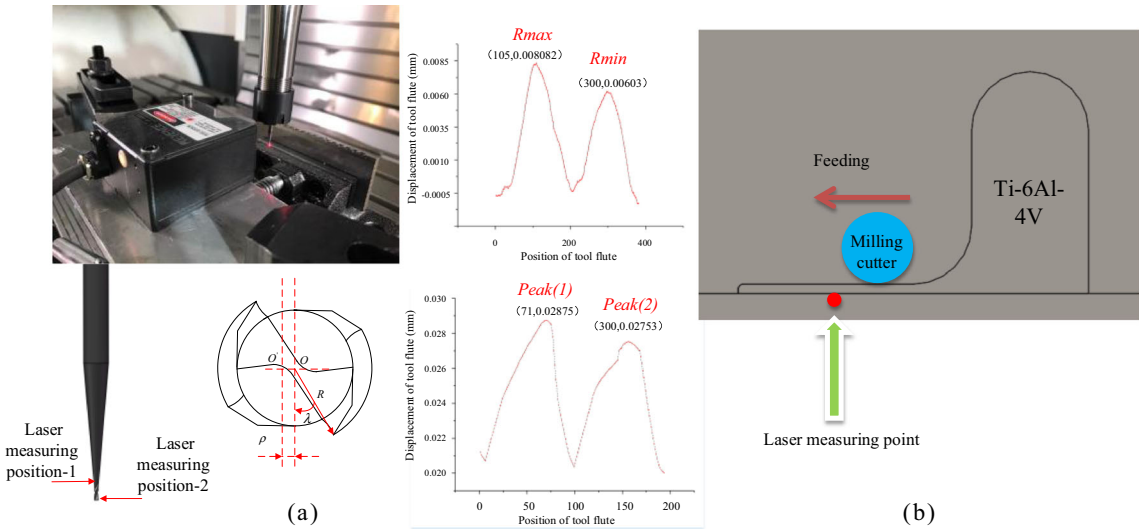

Fig. 9 Laser measuring position. **a** Tool run-out. **b** Deflection of micro-thin wall

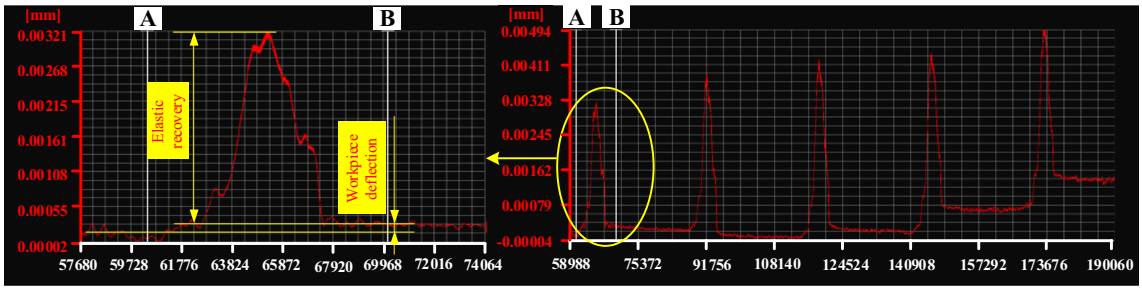

Fig. 10 Post-processing of the deflection of micro-thin wall

With the temperature determined, one of the most significant characteristics in the micro-machining, material strengthening on the flow stress can therefore be accounted for with a modified J-C constitutive model developed by introducing effective strain gradient based on the Taylor's dislocation model, whose expression is given as follows:

$$\tau = \frac{1}{M}\sigma_{JC}\sqrt{1+\left(\frac{M^2\bar{r}\alpha_t^2 G^2 b\eta}{\sigma_{JC}^2}\right)^u}. \tag{28}$$

where M, the Taylor factor, is taken as 3.1 under the assumption that the Taylor factor applied in this model can be reflected by the average values of the Taylor factor of all grains in the polycrystalline metal alloy Ti-6Al-4V [25]. $\bar{r}$, the Nye factor, is taken as 2 [26]. G, the shear modulus, is taken as 44 GPa. b, the magnitude of the Burgers vector, is taken as 0.270 nm [27]. The empirical coefficient α_t and the exponential factor u are both taken as 0.5, while the strain gradient η [28] is expressed as follows:

$$\eta = \frac{\sin\phi_n}{h}. \tag{29}$$

2.3.2 Calculation of micro-flank milling forces

Now that the plowing force coefficients, K_{te} and K_{re}, and the shearing force coefficients, K_{tc} and K_{rc}, are determined through the calculations introduced above. Integrating the differential orthogonal micro-flank milling forces of the feed (x) direction dF_x and transverse (y) direction dF_y from the entry angle α_{in} to the exit angle α_{ex} of each cut and adding up the micro-flank milling forces of each individual flute, the cutting force expressions can be expressed as:

$$\begin{cases} F_x = \dfrac{d_2}{2\tan\lambda_s}\sum_0^{K-1}\int[K_{te}\cos\varphi + K_{re}\sin\varphi + (K_{te}\cos\varphi + K_{rc}\sin\varphi)h]d\varphi \\ F_y = \dfrac{d_2}{2\tan\lambda_s}\sum_0^{K-1}\int[-K_{te}\cos\varphi + K_{re}\sin\varphi + (-K_{te}\cos\varphi + K_{rc}\sin\varphi)h]d\varphi \end{cases}. \tag{30}$$

2.3.3 Entry angle and exit angle determination

Embracing flank up-milling in this current model, the cutting process is asymmetric for both of the two teeth on the micro-end mill. According to Rodríguez and Labarga [7], the entry angle can be deduced by considering the minimum chip thickness, and the expression for the chip thickness in up-milling developed by Boothroyd and Knight [29], their expression for the entry angle of the first tooth to participate in cutting, is as follows:

$$\alpha_{in1} = \arcsin\frac{\lambda_c r_e}{2f_z}. \tag{31}$$

The entry angle for the second tooth the tip of whose helix is directly opposite to that of the first tooth is π radian larger, so the expression is as follows:

$$\alpha_{in2} = \pi + \arcsin\frac{\lambda_c r_e}{2f_z}. \tag{32}$$

Table 6 The first layer deflection of micro-thin wall

Thickness (μm)	70	80	90	100	150	200	250	300	350	400
Deflection (μm)	3.1	2.45	2.04	1.23	1.02	0.91	0.87	0.81	0.74	0.67

Table 7 Micro-milling parameters and levels assigned for trial

Process parameters	Milling speed v_c (m/min)	Feed per tooth f_z (μm/tooth)	Depth of cut per pass a_p (μm)	Depth of cut in radial a_e (μm)
Finishing	25.12	5	200	40

The exit angle of the two teeth of the micro-end mill is co-determined by the combined deformation of the tool and the workpiece at the contacting point of the particular tooth in depth of that tooth. The derived expressions are as follows:

$$\alpha_{ex1} = \arccos\left(\frac{a_e - d_{w1} + \frac{d\cos\alpha_{in1}}{2}}{0.5d}\right) \tag{33}$$

$$\alpha_{ex2} = \pi + \arccos\left(\frac{a_e - d_{w2} + \frac{d\cos\alpha_{in2}}{2}}{0.5d}\right). \tag{34}$$

At the contacting point of the first tooth, the workpiece deformation is d_{w1}; at the contacting point of the second tooth, the workpiece deformation is d_{w2}. Since when the teeth of the micro-end mill exit the flank up-milling process, the orthorhombic milling forces turn zero; a component of those forces, given as F_y in Eq. (8) and Eq. (9), which actuates that the combined deformation of the tool and workpiece can be taken as a minuscule value greater than zero, in this case 0.001 N.

2.4 Experimental set-up

In order to validate the accuracy of the model of the proposed micro-end milling forces, micro-thin-walled part experiments were carried out by a DMU 80 mono BLOCK milling center. It possesses five axes, a maximum spindle speed of 24,000 r/min, a maximum spindle power of 26 kW, a maximum feed rate of 30 m/min, an axial positioning accuracy of 0.008 mm, and a maximum stroke of 980 mm × 630 mm × 630 mm. The zero-reference surface of workpiece was machined to reduce the error of micro-thin-walled depth in the radial and axial directions. Figure 5 illustrates the basic experimental set-up.

The workpiece material tested in this study is Ti-6Al-4V titanium alloy whose physical properties are shown in Table 2 and whose chemical compositions are provided by the manufacturer in Table 3.

The delamination turning is widely used in the trapezoidal thread machining process. In this research, the delamination micro-milling was introduced to manufacture the micro-thin wall under mesoscale. In order to guarantee the thickness precision of micro-thin wall and reduce the effect of weak stiffness, the tool trajectories (Fig. 6) of finish machining were separated into five layers using the software Power-mill.

A German made KENAMETAL carbide flat micro-milling cutter (Fig. 7) with two edges was employed to machine the micro-thin wall. The basic parameters of micro-milling cutter are indicated in Table 4.

2.5 Instruments and measuring methods

The micro-milling forces in the x- and y-directions affected by the deflection of thin wall were measured with the Kistler dynamometer 9119AA2 during the micro-milling experiment. The mechanical parameters of the dynamometer are summarized in Table 5. The workpiece was installed on the Kistler dynamometer, and NI data acquiring system was used to collect and record the milling forces through a Kistler 8 channel charge amplifier with a data sampling rate of 10,000 Hz. Figure 8 shows the post-processing of micro-milling forces. The force signals were filtered at a frequency lower than the system natural frequency to avoid self-excited vibrations.

The measurements of tool run-out and deflection of thin wall were performed by Keyence LK-H020 laser sensor. As shown in Fig. 9a, the extreme displacement of the tool shank (position 1), the maximum and minimum (R_{max} and R_{min}), is obtained by using the laser displacement sensor when rotating the spindle one revolution, and the offset distance ρ can be calculated by [11]:

$$\rho = \frac{R_{max} - R_{min}}{2}. \tag{35}$$

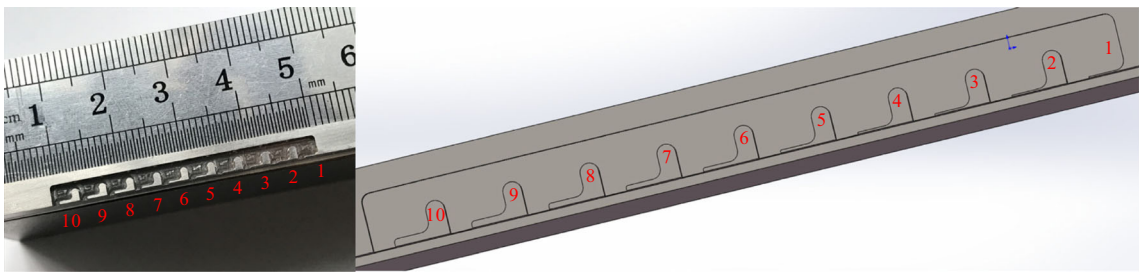

Fig. 11 Machined and 3D designed diagram of micro-thin walls

Table 8 Micro-thin-walled shape and size characteristics

Micro-thin wall	1	2	3	4	5	6	7	8	9	10
Thickness h_w (μm)	70	80	90	100	150	200	250	300	350	400
Height h (mm)	1	1	1	1	1	1	1	1	1	1

The offset direction angle λ is obtained by:

$$peak(1)-peak(2) = \sqrt{R^2+\rho^2-2R\rho\cos(-\lambda)} - \sqrt{R^2+\rho^2-2R\rho\cos\left(\frac{2\pi}{N_t}-\lambda\right)}. \quad (36)$$

The displacement of tool tip in the position 2, that is peak (1) and peak (2) can be measured using the laser sensor. Then offset direction angle λ can be calculated.

Illustrated in Fig. 9b, the laser measuring point is at the top and middle of each micro-thin wall. Figure 10 shows the post-processing of the measured deflection of micro-thin wall, and the results are in Table 6, from which the elastic and plastic deformation were inflicted on micro-thin wall during micro-milling process.

2.6 Micro-milling condition

Spindle speed (n), feed per tooth (f_z), depth of cut per pass (a_p), and radial depth of cut (a_e) were considered as micro-milling parameters. Up-milling and air-cooling are used on the micro-thin walls. Moreover, the depth of cut in radial is very little (40 μm) and the effective diameter of the micro-milling cutter decrease (0.875 μm) is very small, so the tool wear can be ignored. The tool manufacturing company recommended the values of these parameters. The variable factors in this research are summarized in Table 7. In this experiment, ten micro-thin walls had been machined. Figure 11 shows the serial number and location of the micro-thin walls. In addition, Table 8 illustrates the shape and size characteristics micro-thin-wall design.

3 Results and discussions

3.1 Milling forces of micro-thin wall with different thickness

The purpose on studying micro-flank milling forces is to understand its mechanisms and to find its factors of influence during the flank milling of micro-impellers. Focusing on the deflection and size precision of micro-thin wall, the average amplitude of maximum micro-flank milling forces in five cycles is taken as the evaluation criterion. The predicted micro-flank milling forces considering the tool run-out and material strengthening and both the deflection of the tool and thin wall are compared with the experimental measurements to validate the effectiveness of the proposed model. The experimental and predicted results of micro-flank milling forces at the top section of the middle of the thin wall are listed in Table 9. From Table 9, the proposed model performs well for the micro-flank milling forces in the x-direction, with the average error of 4.153%; in the y-direction, the average error is slightly smaller at 4.458%. Also, the maximum error does not exceed 7.109% in the x-direction and 7.112% in the y-direction. Additionally, the minimum error reaches 3.028 and 3.092% in the x- and y-directions, accordingly. The predicted micro-flank milling forces and experimental measurements are

Table 9 Comparison of micro-flank milling forces of micro-thin walls in x- and y-directions

Designed thickness of thin wall (μm)	Average amplitude of maximum micro-flank milling forces (N)					
	F_x			F_y		
	Experimental value (N)	Predicted value (N)	Error (%)	Experimental value (N)	Predicted value (N)	Error (%)
70	− 2.293	− 2.13	7.109	1.631	1.515	7.112
80	− 2.457	− 2.301	6.349	1.738	1.624	6.559
90	− 2.546	− 2.41	5.342	1.849	1.751	5.300
100	− 2.675	− 2.594	3.028	2.167	2.1	3.092
150	− 2.736	− 2.651	3.107	2.296	2.216	3.484
200	− 2.751	− 2.665	3.126	2.393	2.301	3.845
250	− 2.792	− 2.7	3.295	2.482	2.385	3.908
300	− 2.821	− 2.72	3.580	2.555	2.46	3.718
350	− 2.844	− 2.752	3.235	2.642	2.538	3.936
400	− 2.887	− 2.79	3.360	2.678	2.581	3.622
Average			4.153			4.458

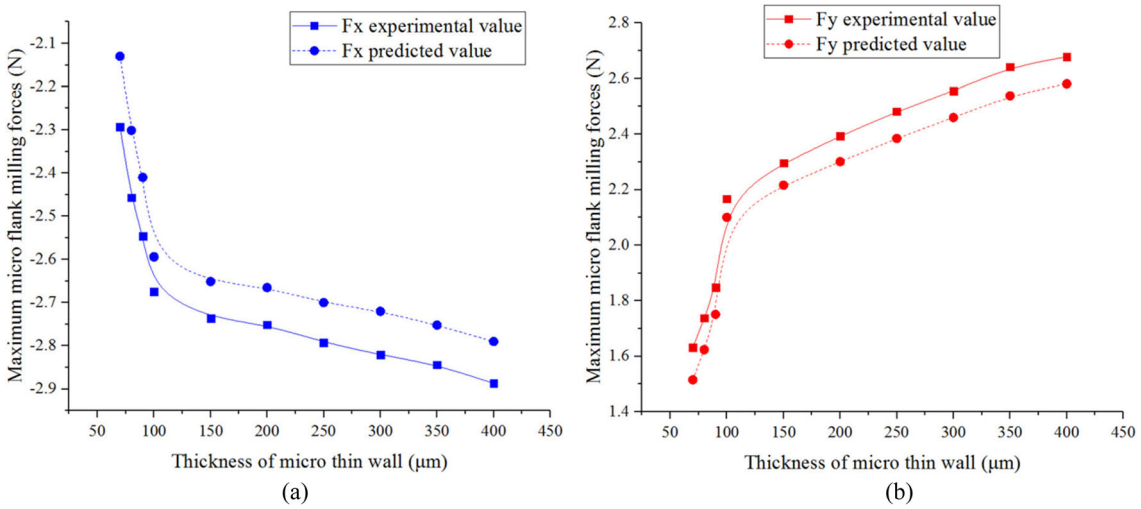

Fig. 12 Comparison of experimental and predicted micro-flank milling forces of finishing machining thin wall. **a** F_x, **b** F_y (v_c = 25.12 m/min, f_z = 5 μm/tooth, a_p = 200 μm, a_e = 40 μm)

shown in Fig. 12a. F_x is the milling force in the feeding direction and Fig. 12b. F_y is the milling force in vertical to the thin wall before its deformation. Figure 13 illustrates the predicted error of micro-flank milling forces in the *x*- and *y*-directions. In terms of micro-milling forces by finishing machining, the predicted micro-flank milling forces by the proposed model have good agreements with the experimental measurements of all cases. However, the predicted micro-flank milling forces are a little less than those measured by experiments because the effects of elastic recovery are not considered in the analytical model of micro-flank milling forces. Besides, there is an obvious phenomenon that the micro-flank milling forces in the *x*- and *y*-directions decreased drastically as the thickness of micro-thin wall becoming smaller gradually when the micro-thin wall is thinner than 100 μm. Nevertheless, when the micro-thin wall is thicker than 100 μm, the micro-flank milling forces in *x*- and *y*-directions increase slowly as the thickness of micro-thin wall gradually increases. This can be explained by the fact that the deflection of micro-cutting tools and thin wall gradually increases as the thickness of micro-thin wall decreases. This phenomenon can lay a feasible foundation for improving the machining precision of micro-thin wall through methods of adjusting micro-flank milling forces.

3.2 Effect of whole deflection of tool and thin wall on micro-flank milling forces

It is generally known that the deflection of tool has a remarkable effect on micro-flank milling forces in micro-end milling process. However, the deflection of workpiece also has a significant influence on micro-flank milling forces when the

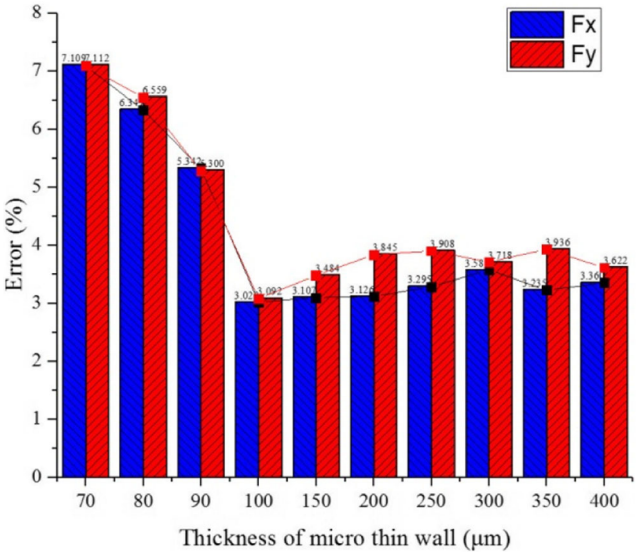

Fig. 13 Predicted error of micro-flank milling forces

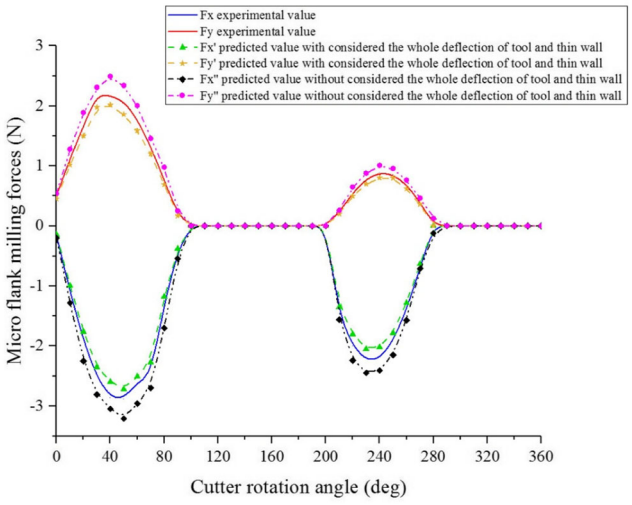

Fig. 14 Predicted micro-flank milling forces with and without the whole deflection of tool and thin wall considering the tool run-out and material strengthening (v_c = 25.12 m/min, f_z = 5 μm/tooth, a_p = 200 μm, a_e = 40 μm, h_w = 100 μm)

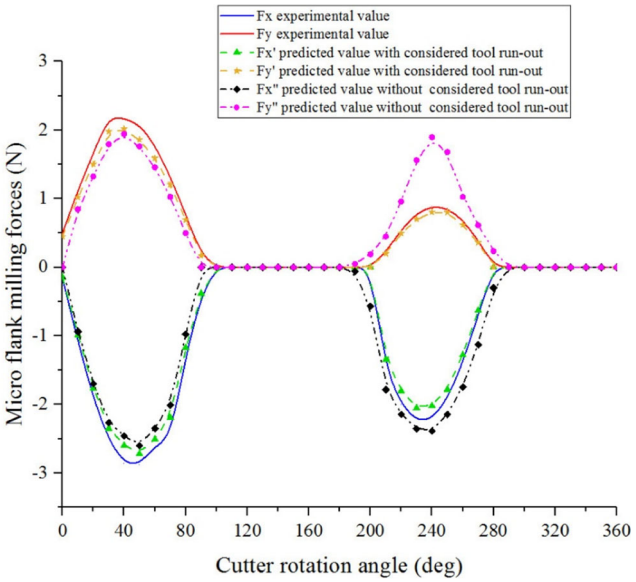

Fig. 15 Predicted micro-flank milling forces with and without considered tool run-out (1.026 μm) considering the whole deflection of tool and thin wall and material strengthening (v_c = 25.12 m/min, f_z = 5 μm/tooth, a_p = 200 μm, a_e = 40 μm, h_w = 100 μm)

width of micro-thin wall decreased to a sufficiently thin extent. In Fig. 14, F_x' and F_y' represent the micro-flank milling forces considering the deflection of tool and thin wall in *x*- and *y*-directions, separately, while F_x'' and F_y'' are the micro-flank milling forces without considering both the deflection of the tool and the thin wall in the *x*- and *y*-directions, and F_x and F_y are the micro-flank milling forces obtained from experiments. The thickness of the thin wall is 100 μm. Besides, Fig. 15 also shows that the single-edge cutting phenomenon occurs when the depth of cut in radial direction is less than $0.5d_2$ during the flank milling micro-thin-walled parts. The reason is the immerse angle between cutting tool and workpiece is less than 90° and it is less than the intersection angle between the two teeth of micro-milling cutter. The simulated results show that the whole deflection of tool and thin wall leads to a slightly decrease in the magnitude of the micro-flank milling forces in both the *x*- and *y*-directions. Without considering the deflection of both the tool and the workpiece, the magnitude of the simulated forces is larger than the experimental milling forces. When considering the deformation of both the tool and the workpiece, the average difference between the simulated results and experimental micro-flank milling forces is about 8.303 and 9.607% in *x*- and *y*-directions, respectively, while for simulations without considering deflection, the average difference is around 13.925 and 14.967% in *x*- and *y*-directions, respectively. For both flutes, the micro-flank milling forces considering the whole deflection of tool and thin wall have better agreement with the experimental results compared to those without considering the whole deflection of tool and thin wall.

3.3 Effect of tool run-out on micro-flank milling forces

Besides deformation, another critical issue affecting the machining precision problem during the micro-milling process is the tool run-out. Tool run-out often occurs in the micro-milling of thin walled parts. Figure 15 depicts the influence of tool run-out. In Fig. 15, the predicted micro-flank milling forces differ for two flutes with and without considered run-out (1 μm). F_x' and F_y' represent the micro-flank milling forces when a tool run-out offset of 1 μm in the *x*- and *y*-directions is separately taken into consideration, while F_x'' and F_y'' correspond to no run-out in both the *x*- and *y*-directions. F_x and F_y are the micro-flank milling forces obtained from experiments. Comparing with the experimental value of micro-forces, when considering tool run-out, the average difference for both flutes is 8.313% in *x*-direction and 9.607% in *y*-direction; when not considering tool run-out, the average difference for both flutes is 16.843% in *x*-direction and 50.15% in *y*-direction. So, the predicted micro-flank milling

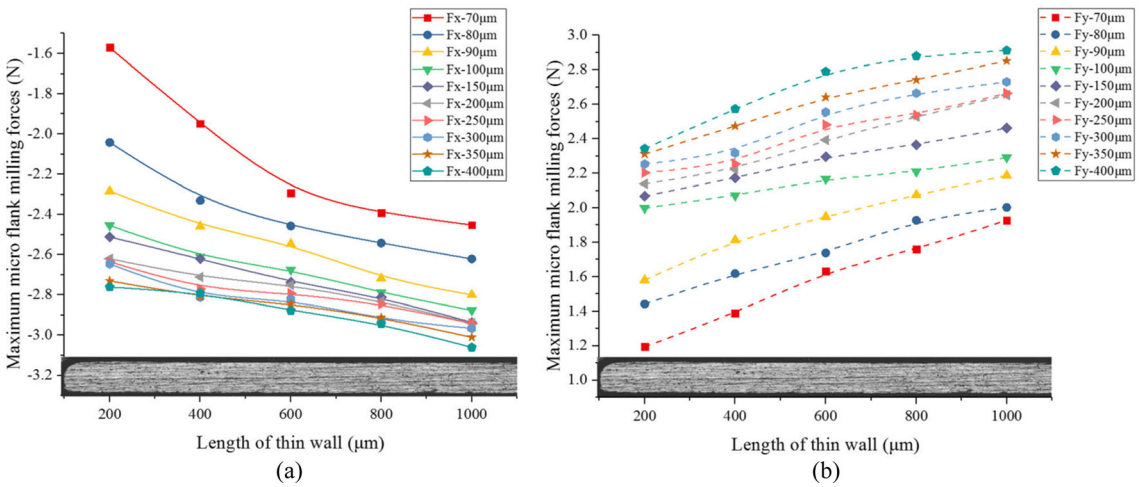

Fig. 16 Micro-flank milling forces in different locations of thin wall with different thicknesses

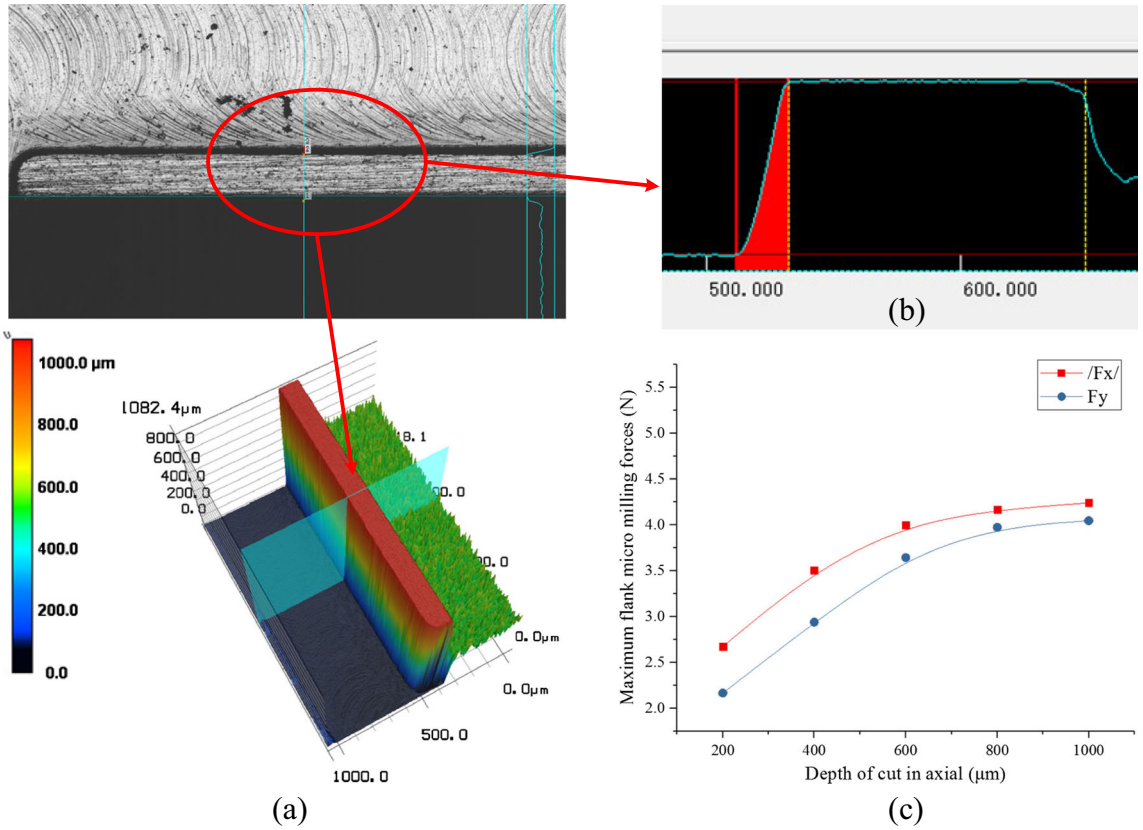

Fig. 17 Topography of machined thin wall and micro-flank milling forces of different depth of cut in axial

forces which takes tool run-out into consideration is closer the actual experimental values. Compared to the influence of both the deflection of tool and thin wall in Fig. 14, the micro-flank milling forces slightly decrease and the average difference becomes larger because of tool run-out, which means that the effects of both the deflection of tool and thin wall on predicted micro-flank milling forces are pronounced.

3.4 Effect of stiffness on micro-flank milling forces

The stiffness at different locations on the thin wall is another factor that affects the micro-flank milling forces of the thin wall. Figure 16a and b presents the micro-flank milling forces F_x and F_y on different locations of thin wall with different thicknesses. As the width of thin wall increases from 100 to 400 μm, the micro-flank milling forces of thin wall gradually became larger in the *x*- and *y*-directions, while when the thickness of thin wall increases from 70 to 90 μm, the micro-flank milling forces increases drastically. Though the micro-flank milling forces are hard to control, future research is required to investigate better methods for micro-force milling adjustment to improve the precision of micro-milled thin walls.

Figure17a and b represents the 3D and 2D topography of machined thin wall. Figure 17c depicts the micro-flank milling forces under different axial depths of cut. The micro-flank milling forces in the *x*- and *y*-directions slowly became larger as the depth of cut in the axial direction increased. As shown in Fig. 17b, the cross section of thin wall is trapezoidal like. Thus, the discussion above suggests that during delamination micro-milling, the material of a front layer can be removed partially by the milling of the next layer. This verified the pattern of the instantaneous micro-flank milling forces, as shown in Fig. 17c.

4 Conclusions

During the milling process, due to the fact that the laser spot cannot move along with the milling cutter for measurement and the deformation of cutting tool and thin wall during the first layer of cutting can be accurately measured with the Keyence LK-H020 laser sensor, this article focuses on the micro-milling force at the middle position of thin wall during the first layer of mesoscale machining. The influence of tool wear is ignored because a new milling cutter with sharp cutting edges was used and the wear measured after the experiments was found to be negligible. In this work, a novel micro-flank milling force prediction model has been presented. The advantage of the developed model is that it takes the tool and workpiece deflection, tool run-out, and material strengthening effects into account during the flank milling of thin-walled parts. Besides, model of the cutting tool is a more accurate

resemblance of the actual structure and the deflection of the model is established on the Euler Bernoulli cantilever beam theory under mesoscale. The mechanistic model is validated by a series of micro-thin-wall experiments with a two-flute KENNA micro-end mill as tool and Ti-6Al-4V titanium alloy as workpiece material. The conclusions can be drawn as follows:

(a) In terms of micro-flank milling forces by finishing machining under mesoscale. For all cases, the predicted micro-flank milling forces of the proposed model have good agreements with the experimental values. The amplitude of micro-flank milling forces in *x*-direction is a little larger than that in the *y*-direction. Experimental results illustrate that the proposed model performs well for calculating the micro-flank milling forces in the *x*-direction with an average error of 4.153%, while slightly larger in the *y*-direction with an average error of 4.458%.

(b) The single-edge cutting phenomenon occurs when the depth of cut in radial direction is less than $0.5d_2$ during the flank milling of micro-thin-walled parts. The simulated results show the total deflection of the tool and thin wall leads to a slight decrease in the magnitude of the micro-flank milling forces both in the *x*- and *y*-directions. For both flutes, when considering the total deflection of tool and thin wall, the micro-flank milling forces predicted by the theoretical model have a better agreement with the experimental results, compared to the calculations made without considering the total deflection of tool and thin wall.

(c) When considering the tool run-out, the predicted micro-flank milling forces correspond closely with the actual experimental values.

(d) The micro-flank milling forces in the *x*- and *y*-directions gradually became larger as the depth of cut in axial increased. During delamination micro-milling, the material of a front layer can be removed partially by milling the next layer.

Funding information The authors wish to acknowledge the financial support for this research from the National Natural Science Foundation of China (Item nos. 51575050 and 51505034).

References

1. Chae J, Park SS, Freiheit T (2006) Investigation of micro-cutting operations. Int J Mach Tools Manuf 46(3–4):313–332
2. Yasaitis JA (2001) Progress and profit through microtechnologies: commercial applications of MEMS/MOEMS micromachining and microfabrication. Proc Spie 4557:1–10
3. Tosello G, Bissacco G, Tang PT, Hansen HN, Nielsen PC (2008) High aspect ratio micro tool manufacturing for polymer replication using μEDM of silicon, selective etching and electroforming. Microsyst Technol 14:1757–1764
4. Bissacco G, Hansen HN, Slunsky J (2008) Modelling the cutting edge radius size effect for force prediction in micro milling. CIRP Ann Manuf Technol 57(1):113–116
5. Park SS, Malekian M (2009) Mechanistic modeling and accurate measurement of micro end milling forces. CIRP Ann Manuf Technol 58(1):49–52
6. Malekian M, Park SS, Jun MBG (2009) Modeling of dynamic micro-milling cutting forces. Int J Mach Tools Manuf 49(7):586–598
7. Rodríguez P, Labarga JE (2013) A new model for the prediction of cutting forces in micro-end-milling operations. J Mater Process Technol 213(2):261–268
8. Jing XB, Tian YL, Yuan YJ, Wang FJ (2017) A runout measuring method using modeling and simulation cutting force in micro end-milling. Int J Adv Manuf Technol 91(9–12):4191–4201
9. Mamedov ASELK, Lazoglu I (2013) Machining forces and tool deflections in micromilling. Procedia Cirp 8:147–151
10. Zhang XW, Ehmann KF, TB Y, Wang WS (2016) Cutting forces in micro-end-milling processes. Int J Mach Tools Manuf 107:21–40
11. Zhang DL, Mo R, Chang ZG, Sun HB, Li CL (2016) A study of computing accuracy of calibrating cutting force coefficients and run-out parameters in flat-end milling. Int J Adv Manuf Technol 84(1–4):621–630
12. Joshi SS, Melkote SN (2004) An explanation for the size-effect in machining using strain gradient plasticity. J Manuf Sci Eng Trans ASME 126(4):679–684
13. Liu K, Melkote SN (2006) Material strengthening mechanisms and their contribution to size effect in micro-cutting. Trans. Manuf Sci Eng Trans ASME 128(3):1147–1156
14. Srinivasa YV, Shunmugam MS (2013) Mechanistic model for prediction of cutting forces in micro end-milling and experimental comparison. Int J Mach Tools Manuf 67(2):18–27
15. Zhou L, Peng FY, Yan R, Yao PF, Yang CC, Li B (2015) Analytical modeling and experimental validation of micro end-milling cutting forces considering edge radius and material strengthening effects. Int J Mach Tools Manuf 97:29–41
16. Wang J, Tang S, Jiang L (2007) Plate & Shell Mechanics Problem-Solving Guidance. Tongji University Press, Shanghai
17. Zhang WH, Wan M (2016) Milling simulation metal milling mechanics, dynamics and clamping principles. Northwestern Polytechnical University Press, Xi'an, p 272
18. Yongqing W, Haibo L (2011) A novel mechanics model of parametric helical-end mills for 3D cutting force prediction. Proc Inst Mech Eng C J Mech Eng Sci 1989–1996 (vols 203–210) 225(7): 1693–1702
19. Mijušković G, Krajnik P, Kopač J (2015) Analysis of tool deflection in micromilling of graphite electrodes. Int J Adv Manuf Technol 76(1):209–217
20. Basuray PK, Misra BK, Lal GK (1977) Transition from ploughing to cutting during machining with blunt tools. Wear 43(3):341–349
21. Manjunathaiah J, Manjunathaiah J (1998) Analysis and a new model for the orthogonal machining process in the presence of edge-radiused (non-sharp) tools. Dissertation, University of Michigan
22. Abdelmoneim ME, Scrutton RF (1974) Tool edge roundness and stable build-up formation in finish machining. J Eng Ind 96(4): 1258–1267
23. Chen G, Ren C, Yang X, Jin X, Guo T (2011) Finite element simulation of high-speed machining of titanium alloy (Tl–6Al–4V) based on ductile failure model. Int J Adv Manuf Technol 56(9):1027–1038
24. Tounsi N, Vincenti J, Otho A, Elbestawi MA (2002) From the basic mechanics of orthogonal metal cutting toward the identification of the constitutive equation. Int J Mach Tools Manuf 42(12):1373–1383

25. Clausen B, Riso F, Højskole DT (1997) Characterisation of polycrystal deformation by numerical modeling and neutron diffraction measurements. Dissertation, Technical University of Denmark
26. Gao H, Huang Y (2001) Taylor-based nonlocal theory of plasticity. International Journal of Solids & Structures 38(15):2615–2637
27. Gao Y (2010) Effect of shot-peening on microstructure of TC4 titanium alloy. Rare Metal Materials & Engineering 39(9):1536–1539
28. Joshi SS, Melkote SN (2004) An explanation for the size-effect in machining using strain gradient plasticity. J Manuf Sci Eng 126(4):679–684
29. Boothroyd G, Knight WA (2010) Fundamentals of machining and machine tools. Marcel Dekker Inc., New York City